Acta Mech 233, 2061–2075 (2022)
https://doi.org/10.1007/s00707-022-03170-1

ORIGINAL PAPER

Fujun Jiang · Min Yu · Xianghua Peng · P. H. Wen

Effect of nanoscale amorphization in nanocrystalline bimaterials on dislocation emission from the tip of colinear linear cracks

Received: 24 October 2021 / Revised: 13 December 2021 / Accepted: 12 February 2022 / Published online: 10 May 2022

Abstract In this paper, a theoretical model is established to describe the effect of nanoscale amorphization in nanocrystalline bimaterials on the dislocation emission from the tip of a collinear crack at the interface. In the description, nanoscale amorphization is formed by the splitting transition of the Grain Boundary (GB, the disclination of GBs caused by the movement of GBs). The analytical solution of the model is obtained by the elasticity complex potential solution method. In addition, the effects of nanoscale amorphization, dislocation emission angle, interfacial crack length and material constants of nanocrystalline bimaterials on the critical stress intensity factor of interfacial crack tip corresponding to dislocation emission are discussed through numerical analysis. The analysis shows that the influence of nanoscale amorphization in nanocrystalline bimaterials on the critical stress intensity factor (SIF) corresponding to dislocation emission depends on the dislocation emission angle, the position and size of the nanoscale amorphization, interface crack length and relative shear modulus. With the increase in relative shear modulus and dislocation emission angle, the normalized critical SIF decreases at first and increases afterwards. When the nanoscale amorphization size is small, the critical SIF of the dislocation is less affected, but when the size is larger, the impact becomes great. The influence of nanoscale amorphization on the dislocation emission from collinear interface crack tip is related to nanoscale amorphization and relative shear modulus. There is a critical relative shear modulus that the increase in dislocation intensity has little effect on dislocation emission. Appropriate selection of materials for the upper and lower planes can reduce the critical stress intensity factor corresponding to dislocation emission, thereby promoting the dislocation emission from interface cracks and improving the toughness of the nanocrystalline bimaterials.

1 Introduction

Nanocrystalline materials have the characteristics of high resistivity, good biocompatibility, high strength, low density, etc., and show a wide range and significant development prospects in the application of micro-/nanotechnology [1–5]. Although the strength and hardness of nanocrystalline and ultrafine particle materials are 2–10 times those of traditional coarse-grained materials [6], the shortcomings of low tensile ductility and low fracture toughness at room temperature severely limit their practical applications. Therefore, in order to

F. Jiang · M. Yu (✉)
College of Civil Engineering, Central South University of Forestry and Technology, Changsha 410004, People's Republic of China
e-mail: yumin1999@163.com

X. Peng (✉)
College of Information Science and Engineering, Hunan Women's University, Changsha 410004, People's Republic of China
e-mail: pxh10000@163.com

P. H. Wen
School of Engineering and Material Sciences, University of London, London E1 4NS, Queen Mary, UK

solve this problem, researchers used a lot of advanced material preparation technology to improve the fracture toughness of nanocrystalline ceramics [7–10]. When studying the toughening micro-mechanism that plays an important role in nanocrystalline and ultrafine particle materials, the researchers found that the specific properties of nanocrystalline materials are controlled by their specific structural characteristics, such as a large number of GB [11], GB movement [12], GB migration [13], diffusion creep, cooperative dislocation [14], rotational deformation [15] and nanoscale twin deformation [16], etc. Alternative deformation modes can effectively act on nanocrystals and ultrafine particles [17], and these will lead to the operation of specific structural deformation and fracture mechanisms.

In recent years, the special deformation mechanism of nanoscale amorphization (the formation of nanoscale amorphized regions) in deformed nanocrystalline and ultrafine particle materials observed in experiments has attracted widespread attention from scholars [18, 19]. A large number of experiments [20], theoretical models [21] and computer simulations [22] have proved that nanoscale amorphization can effectively occur in nanocrystalline and polycrystalline materials [23, 24]. It is found in experiments that the local amorphization near crack tips will affect crack propagation of conventional coarse-grained materials [25]. And computer simulations [26] and theoretical analysis [27] show that nanoscale amorphization can effectively occur in GBs and at the triple junction, which is a process driven by lattice relaxation. In the absence of any external mechanical load, nanoscale amorphization can effectively occur at the GB and its triple junction, which is a process driven by the elastic energy relaxation of the GB disclination (line defects related to sudden changes in GB direction/gap [28]). Generally, the high local stress near the crack tip causes the GB to slip. And, through the splitting and conversion of GB disclinations produced by GB slippage, nanoscale amorphization can occur [6]. Researchers have found that nanoscale amorphization may be used as a special deformation mode for initially deformed materials under various applied stresses [29]. Ovid'ko and Sheinerman [30] established a theoretical model of the amorphization process and studied the effects of GBs and crack passivation on the fracture toughness of nanocrystalline and ultrafine grained materials. As a result, they found that nanoscale amorphization can occur on GB dipoles, and they used nanoscale amorphization as a special deformation method to act as local plasticity near the crack tip [6].

As we all know, the dislocation emission from the crack tip is one of the most basic processes to understand the crack passivation of nanocrystalline and ultrafine particle materials. Once the dislocations are released, they move out of the crack tip area, leaving a dislocation-free area. The internal stress which is caused by the dislocations generated at the crack tip adapts the stress intensity factor to the applied load, thereby enhances the fracture toughness of the material. D Lyu [31] understands the dislocation mode and its relationship with the macro-mechanical properties from the perspective of dynamics. The dislocation mode has a significant and decisive effect on work hardening and plastic strain localization, while the dislocation microstructure affects the macro-scale material properties. Fang [32] pointed out that the GB sliding deformation mechanism is very effective in increasing the critical SIF of the finest grain crack propagation in nanocrystalline materials, and GB sliding deformation can increase the number of dislocations emitted by the crack tip, thereby enhancing the toughness of the material. Zhou K [33] pointed out in the article that the position of the dislocation has a significant effect on the image force acting on the dislocation, which depends on the elastic constant of the material. Typically, the crack blunting and growth process are controlled by the dislocation emission from the crack tip. According to their description, both crack blunting and dislocation stress field hinder the crack from further releasing dislocations. As a result, the reduction in particle size causes nanocrystalline and ultrafine particle materials to exhibit brittleness. In fact, the dislocation release has a profound effect on the number of dislocations released at the crack tip and the fracture toughness of nanocrystalline and ultrafine crystalline materials.

Nanocrystalline bimaterials are more prone to interface cracks initiating near the bonding surface and expanding along the interface until the structure breaks. Therefore, the failure of nanocrystalline bimaterials is not only the problem of cracks inside a single material, but also of the failure of the interface or near the interface. With the continuous development of computational mechanics, numerical calculation methods for solving fracture mechanics problems continue to emerge, and they have become important tools to promote the continuous development of fracture mechanics research. Lee and Huang [34] studied the interference effects of threading dislocations and linear interface cracks from the edges of semi-elliptical holes. Fang et al. [35] studied the interaction between screw dislocations and elastic elliptical inclusions with interfacial cracks. Qiu et al. [36] studied the relationship between the crack length at the interface and the stress component and the value of the electric field intensity in the analysis of the interface crack stress and electric field concentration factor of the film substrate structure. Li Junlin et al. [37] pointed out that the problem of interfacial cracks was transformed into a kind of boundary value problem of generalized reharmonization equations and proposed the

crack tip of the semi-infinite interface of orthotropic bimaterials and the model I, model II and mixed model center penetrating interface, and calculation formulas for crack tip stress intensity factor, stress field and displacement field. Zhao H et al. [38] studied the anti-plane interface crack stress of orthotropic piezoelectric bimaterials and obtained the relationship between the mechanical energy strain release rate and the difference of material parameters, crack length, and applied electromechanical load. Although the current development of computational fracture mechanics is relatively mature, its research on the analysis of bimaterial interface cracks is still lacking, and a lot of research is needed from the perspective of basic research.

In this article, we aim to study how the stress filed generated by nanoscale amorphization in nanocrystalline bimaterials affects the emission of collinear crack tip dislocations at the interface. And we give the basis for judging the first edge dislocation emission from the tip of a collinear linear crack near a nanoscale amorphization in nanocrystalline bimaterials. Numerical examples are used to analyze the influence of nanoscale amorphization, dislocation emission angle, crack length, and relative shear modulus of nanocrystalline bimaterials on the critical stress intensity factor corresponding to dislocation emission, and to get the influence law of nanoscale amorphous on the dislocation emission from the interface crack tip, so as to explore the toughness changes of nanocrystalline bimaterials containing defects due to dislocation emission.

2 Model and basic formula

As shown in Fig. 1, considering an infinite nanocrystalline bimaterial solid that is subjected to in-plane shear load (model II) and tensile load (model I) at infinity, the deformed infinite nanocrystalline bimaterial solid contains a large number of nanoscale crystal grains separated by grain boundaries. Assuming that the interface of the bimaterials is a straight line, there are a series of collinear linear cracks on the interface and a nanoscale amorphous is produced near a certain interface crack attachment. It is assumed that all micro-defects are unchanged along the direction perpendicular to the plane, so the model can be regarded as a plane strain problem. Assuming that the plane is the xy plane, the interface of the bimaterials is set to the x-axis, the part of the complete connection on the interface is represented by L', and the aggregated part of collinear linear cracks with endpoints a_j and b_j existing on the interface $L_j (j = 0, 1, 2, \ldots)$ can be represented as L. Nanocrystalline bimaterials are assumed to be isotropic, and the shear modulus and Poisson's ratio of the upper half plane are μ_1 and ν_1, respectively, and the lower half plane is μ_2 and ν_2.

Two coordinate systems are introduced: the Cartesian coordinate system x', y' with the origin at A and the polar coordinate system (r, θ) with the origin at the right end of the crack L_0, as shown in Fig. 1(b). For solids subjected to external loads, the relaxation of stress is achieved through plastic deformation or failure processes. Therefore, Ovid'ko and Sheinerman [30] believe that the grain boundary dislocations move during their splitting transition, and relax the stress generated by the disclination dipole by forming local plastic deformation. Grain boundary dislocations are not lattice dislocations, and their movement will form a disordered region composed of grain boundary dislocations, called amorphous regions.

For simplicity, it is assumed that lattice dislocations are continuously distributed in the rectangular amorphous region $ABCD$ at a constant density, as shown in Fig. 2c. According to the solid defect theory of Hirth and Lathe [39], continuous and uniform dislocations can be regarded as an array of dislocation walls located between the opposite boundaries (AD and BC) of the amorphous region. Each dislocation wall located between these boundaries can be represented by a wedge disclination dipole. Therefore, the amorphization in the rectangular region can be equivalently represented by n pairs of wedge disclination dipoles uniformly distributed on the side boundaries AD and BC (as shown in Fig. 2d).

Assuming that the sliding direction of the GB is the extension direction of the y' axis, and the expansion direction of the amorphous nucleus is the extension direction of the x' axis, the wedge disclination values on different side boundaries are equal and opposite. $1/s$ represents the linear density of evenly distributed wedge disclinations. The total strength of wedge dislocations on the AD and BC boundaries is represented by ω and $-\omega$, respectively, while d represents the wedge disclination arm length, and α represents the angle between one of arm d and the crack surface, expressed as nanoscale amorphization inclination angle.

For the plane problem, there are only stress components, σ_{xx}, σ_{yy} and σ_{xy}, and displacement components u_x and u_y, which can be expressed by two Muskhelishvili complex potential functions $\Phi(z)$ and $\Psi(z)$ [40]:

$$\sigma_{xx} = \mathrm{Re}\Big[2\Phi(z) - z\overline{\Phi'(z)} - \overline{\Psi(z)}\Big], \tag{1}$$

$$\sigma_{yy} = \mathrm{Re}\Big[2\Phi(z) + z\overline{\Phi'(z)} + \overline{\Psi(z)}\Big], \tag{2}$$

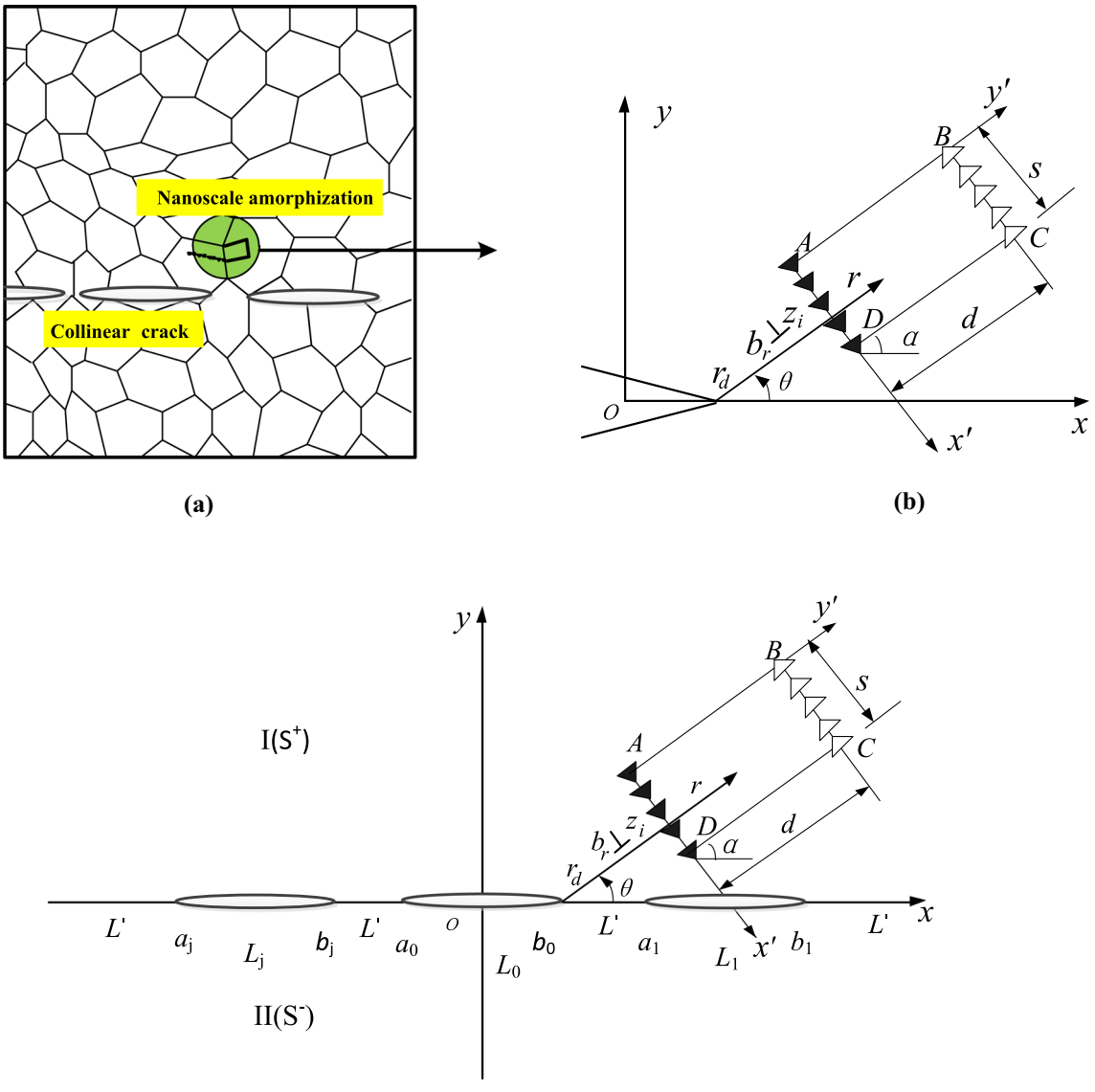

Fig.1 Dislocation emission model of collinear crack tips near a nanoscale amorphization in a nanocrystalline bimaterial solid. **a** General view; **b** Magnified inset highlights of nanoscale amorphization near the tip of a collinear linear crack; **c** Calculation model

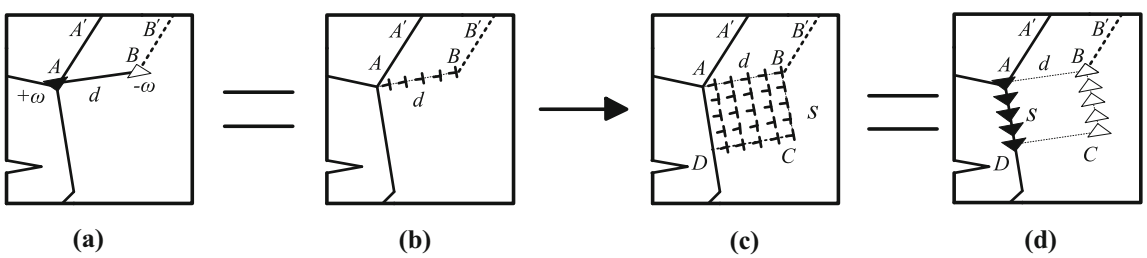

Fig. 2 Formation process of a nanoscale amorphization near the tip of a collinear linear crack in a nanocrystalline bimaterial solid

$$\sigma_{xy} = \mathrm{Im}\left[\overline{z}\Phi'(z) + \Psi(z)\right], \tag{3}$$

$$2\mu(u' + v') = (3 - 4\upsilon)\Phi(z) - \overline{\Phi(z)} - z\overline{\Phi'(z)} - \Psi(z), \tag{4}$$

where z is a complex variable: $z = x + iy$, $\mathrm{i} = \sqrt{-1}$, '—' means complex conjugate, $u' = \partial u/\partial x$, $v' = \partial v/\partial x$, $\Phi'(z) = d\Phi(z)/dz$.

The stress and displacement of the crack-free part of the bimaterial interface are continuous, which can be expressed as:

$$u_1^+(t) + i v_1^+(t) = u_2^-(t) + i v_2^-(t) \quad t \in L', \tag{5}$$

$$\sigma_{yy1}^+(t) - i\sigma_{xy1}^+(t) = \sigma_{yy2}^-(t) - i\sigma_{xy2}^-(t) \quad t \in L'. \tag{6}$$

Among them u_1, v_1 represent the displacement component of the upper half plane, and μ_2, u represent the displacement component of the lower half plane; σ_{xx1}, σ_{yy1} and σ_{xy1}, represent the stress component of the upper half plane, σ_{xx2}, σ_{yy2} and σ_{xy2}, represent the stress component of the lower half plane.

Assuming that the crack surface is free, the boundary condition of collinear crack surfaces can be expressed as:

$$\sigma_{yy1}^+(t) - i\sigma_{xy1}^+(t) = 0 \quad t \in L, \tag{7}$$

$$\sigma_{yy2}^-(t) - i\sigma_{xy2}^-(t) = 0 \quad t \in L. \tag{8}$$

3 The stress field generated by the nanoscale amorphous at the tip of the interface crack

Firstly, let us calculate the stress fields σ_{xx}^{N}, σ_{yy}^{N} and σ_{xy}^{N} generated by the nanoscale amorphous at the tip of the collinear crack in the nanocrystalline bimaterials. A rectangular nanoscale amorphization is produced in the upper half plane at the point $z_k = x_k + iy_k$ near the crack L_0. The nanoscale amorphization area can be equivalently represented by n pairs of wedge disclination dipoles uniformly distributed on the side boundaries AD and BC. Assuming that the stress field generated by a wedge disclination with strength ω is σ_{xx}^D, σ_{yy}^D and σ_{xy}^D, the stress field generated by nanoscale amorphous can be calculated by integration. For example, σ_{xx}^N, can be calculated by the following formula:

$$\sigma_{xx}^N(x, y) = \frac{1}{s}\int_0^s \left(\sigma_{x'x'}^D\left(x', y', x_k', y_k'\right)\Big|_{y_0'=0} - \sigma_{x'x'}^D\left(x', y', x_k', y_k'\right)\Big|_{y_k'=d}\right)dx', \tag{9}$$

where $z = x + iy = x_A + iy_A + \left(x' + iy'\right)e^{i(\alpha-\pi/2)}$.

In the following calculation, when a point $z_k = x_k + \mathrm{i}y_k$ in the upper half plane has a positive wedge disclination with a strength of ω, the stress fields σ_{xx}^D, σ_{yy}^D and σ_{xy}^D produced by it can be calculated by $\Phi_1^D(z)$ and $\Psi_1^D(z)$. The complex potential functions $\Phi_1^D(z)$ and $\Psi_1^D(z)$ in the upper half plane are divided into two parts:

$$\Phi_1^D(z) = \Phi_{10}^D(z) + \Phi_{1*}^D(z) \quad z \in s^+, \tag{10}$$

$$\Psi_1^D(z) = \Psi_{10}^D(z) + \Psi_{1*}^D(z) \quad z \in s^+. \tag{11}$$

Among them, the first parts $\Phi_{10}^D(z)$ and $\Psi_{10}^D(z)$ represent the complex potential function when there is a positive wedge disclination in the upper half plane in an infinite matrix without cracks. The second parts $\Phi_{1*}^D(z)$ and $\Psi_{1*}^D(z)$ represent the complex potential function of the crack interacting with a positive wedge disclination, which is holomorphic in the defined region. From [41]:

$$\Phi_{10}^D(z) = \frac{D_1\omega}{2}\ln(z - z_k) \quad z \in s^+, \tag{12}$$

$$\Psi_{10}^{\omega}(z) = -\frac{D_1\omega}{2}\frac{\overline{z}_k}{z - z_k} \quad z \in s^+. \tag{13}$$

Below we consider the case where there is only a finite-length crack on the interface, without loss of generality, set the crack endpoints as a_0 and b_0, respectively, and finally obtain the complex potential functions $\Phi_1^D(z)$ and $\Psi_1^D(z)$ as [41]:

$$\begin{aligned}\Phi_1^D(z) =& \frac{D_1\omega}{2}\cdot\frac{1-g+h}{1-g}\left(\ln\frac{z-z_k}{z-\overline{z}_k}-\frac{z-z_k}{z-\overline{z}_k}\right)\\ &-\frac{D_1\omega}{2}\cdot\frac{hX_0(z)}{1-g}\cdot\left\{\frac{\ln(z-z_k)}{X_0(z_k)}+g(z_k-\overline{z}_k)-\frac{1}{X_0(\overline{z}_k)}\left[\frac{z-z_k}{z-\overline{z}_k}+\ln(z-\overline{z}_k)\right]\right\},\end{aligned} \tag{14}$$

$$\begin{aligned}\Phi_1^{D\prime}(z) =& \frac{D_1\omega}{2}\cdot\frac{1-g+h}{1-g}\left[\frac{1}{z-z_k}-\frac{2}{z-\overline{z}_k}+\frac{z-z_k}{(z-\overline{z}_k)^2}\right]\\ &-\frac{D_1\omega}{2}\cdot\frac{hX_0'(z)}{1-g}\cdot\left\{\frac{\ln(z-z_k)}{X_0(z_k)}+g(z_k-\overline{z}_k)-\frac{1}{X_0(\overline{z}_k)}\left[\frac{z-z_k}{z-\overline{z}_k}+\ln(z-\overline{z}_k)\right]\right\}\\ &-\frac{D_1\omega}{2}\cdot\frac{hX_0(z)}{1-g}\left\{\frac{1}{X_0(z_k)(z-z_k)}-\frac{1}{X_0(\overline{z}_k)}\left[\frac{2}{z-\overline{z}_k}-\frac{z-z_k}{(z-\overline{z}_k)^2}\right]\right\},\end{aligned} \tag{15}$$

$$\begin{aligned}\Psi_1^D(z) =& -\Phi_1^D(z)-z\overline{\Phi}_1^{D\prime}(z)-\overline{\Phi}_1^D(z)\\ =& -\Phi_1^D(z)-z\overline{\Phi}_1^{D\prime}(z)-\frac{D_1\omega}{2}\cdot\frac{1-g+h}{1-g}\cdot\left[\ln\frac{z-\overline{z}_k}{z-z_k}-\frac{z-\overline{z}_k}{z-z_k}\right]\\ &+\frac{D_1\omega}{2}\cdot\frac{h\overline{X_0}(z)}{1-g}\cdot\left\{\frac{\ln(z-\overline{z}_k)}{\overline{X_0(z_k)}}+g(\overline{z}_k-z_k)-\frac{1}{\overline{X_0(\overline{z}_k)}}\left[\frac{z-\overline{z}_k}{z-z_k}+\ln(z-\overline{z}_k)\right]\right\},\end{aligned} \tag{16}$$

where $D_1=\frac{\mu_1}{2\pi(1-\nu_1)}$, $g=-\frac{\mu_2+\mu_1(3-4\nu_2)}{\mu_1+\mu_2(3-4\nu_1)}$, $h=-\frac{4\mu_2(1-\nu_1)}{\mu_1+\mu_2(3-4\nu_1)}$, $\beta=\frac{\ln|g|}{2\pi}$, $X_0'(z)=\frac{dX_0(z)}{dz}$, $X_0(z)=(z-a_0)^{-0.5-i\beta}(z-b_0)^{-0.5+i\beta}$.

4 Emission of edge dislocations at the tip of a collinear interface crack

Under the action of an external load, the stress concentration at the crack tip will cause dislocations to be emitted from the crack tip. Here, only edge dislocations are considered. Suppose the first edge dislocation reflected by the interface crack is located at a certain point $z_0=b_0+r_0e^{i\theta_0}$ in the upper half plane, and where Burgers vector is $b=b_x-ib_y$. Referring to the literature [42], it can be known that the complex potential functions $\Phi_1^E(z)$ and $\Psi_1^E(z)$ are:

$$\Phi_1^E(z)=\Phi_{10}^E(z)+\Phi_{1*}^E(z)\quad z\in s^+, \tag{17}$$

$$\Psi_1^E(z)=\Psi_{10}^E(z)+\Psi_{1*}^E(z)\quad z\in s^+, \tag{18}$$

where $\Phi_{10}^E(z)=\frac{\gamma_1}{z-z_0}$, $\Psi_{10}^E(z)=\frac{\overline{\gamma}_1}{z-z_0}+\frac{\gamma_1\overline{z}_0}{(z-z_0)^2}$, $\gamma_1=\frac{\mu_1}{4\pi(1-\nu_1)}(b_y-\mathrm{i}b_x)$.

It is known from reference [41] that when there is only a finite-length crack on the interface, without loss of generality, the crack endpoints are also set as a_0 and b_0, and the final complex potential functions $\Phi_1^E(z)$ and $\Psi_1^E(z)$ are:

$$\begin{aligned}\Phi_1^E(z) =& h_1\left[\frac{\gamma_1}{z-z_0}-\frac{\gamma_1}{z-\overline{z}_0}-\frac{\overline{\gamma}_1(z_0-\overline{z}_0)}{(z-\overline{z}_0)^2}\right]+h_2\frac{X_0(z)}{X_0(z_0)}\frac{\gamma_1}{z-z_0}+h_2(1-g)\gamma_1X_0(z)\\ &+h_2\frac{X_0(z)}{X_0(\overline{z}_0)}\left[\frac{\gamma_1}{z-\overline{z}_0}-\frac{\overline{\gamma}_1(\overline{z}_0-z_0)}{(z-\overline{z}_0)^2}-\frac{\overline{z}_0-\frac{1}{2}(a_0+b_0)+i\beta(a_0-b_0)}{(\overline{z}_0-a_0)(\overline{z}_0-b_0)}\frac{\overline{\gamma}_1(\overline{z}_0-z_0)}{(z-\overline{z}_0)}\right],\end{aligned} \tag{19}$$

$$\begin{aligned}\Phi_1^{E\prime}(z) =& h_1\left[-\frac{\gamma_1}{(z-z_0)^2}+\frac{\gamma_1}{(z-\overline{z}_0)^2}+\frac{2\overline{\gamma}_1(z_0-\overline{z}_0)}{(z-\overline{z}_0)^3}\right]+h_2\frac{X_0'(z)}{X_0(z_0)}\frac{\gamma_1}{z-z_0}-h_2\frac{X_0(z)}{X_0(z_0)}\frac{\gamma_1}{(z-z_0)^2}\\ &+h_2\frac{X_0'(z)}{X_0(\overline{z}_0)}\left[\frac{\gamma_1}{z-\overline{z}_0}-\frac{\overline{\gamma}_1(\overline{z}_0-z_0)}{(z-\overline{z}_0)^2}-\frac{\overline{z}_0-\frac{1}{2}(a_0+b_0)+i\beta(a_0-b_0)}{(\overline{z}_0-a_0)(\overline{z}_0-b_0)}\frac{\overline{\gamma}_1(\overline{z}_0-z_0)}{(z-\overline{z}_0)}\right]+h_2(1-g)\gamma_1X_0'(z)\\ &+h_2\frac{X_0(z)}{X_0(\overline{z}_0)}\left[-\frac{\gamma_1}{(z-z_0)^2}+\frac{2\overline{\gamma}_1(\overline{z}_0-z_0)}{(z-\overline{z}_0)^3}+\frac{\overline{z}_0-\frac{1}{2}(a_0+b_0)+i\beta(a_0-b_0)}{(\overline{z}_0-a_0)(\overline{z}_0-b_0)}\frac{\overline{\gamma}_1(\overline{z}_0-z_0)}{(z-\overline{z}_0)^2}\right],\end{aligned} \tag{20}$$

$$\begin{aligned}\Psi_1^E(z) &= -\Phi_1^E(z) - z\overline{\Phi}_1^{E\prime}(z) - \overline{\Phi}_1^E(z)\\ &= -\Phi_1^E(z) - z\overline{\Phi}_1^{E\prime}(z) + h_1\left[\frac{\overline{\gamma}_1}{z-\overline{z}_0} - \frac{\overline{\gamma}_1}{z-z_0} - \frac{\gamma_1(\overline{z}_0-z_0)}{(z-z_0)^2}\right]\\ &\quad + h_2\frac{\overline{X_0}(z)}{\overline{X_0(z_0)}}\frac{\overline{\gamma}_1}{z-\overline{z}_0} + h_2(1-g)\gamma_1\overline{X_0}(z)\\ &\quad + h_2\frac{\overline{X_0}(z)}{\overline{X_0(\overline{z}_0)}}\left[\frac{\overline{\gamma}_1}{z-z_0} - \frac{\gamma_1(z_0-\overline{z}_0)}{(z-z_0)^2} - \frac{z_0-\frac{1}{2}(a_0+b_0)-i\beta(a_0-b_0)}{(z_0-a_0)(z_0-b_0)}\frac{\gamma_1(z_0-\overline{z}_0)}{(z-z_0)}\right],\end{aligned} \tag{21}$$

where $h_1 = \frac{4\mu_1(1-\nu_2)}{\mu_1(1-\nu_2)+\mu_2(1-\nu_1)}$, $h_2 = \frac{4\mu_2(1-\nu_1)}{\mu_1(1-\nu_2)+\mu_2(1-\nu_1)}$.

It can be seen that the total emission force f_{E} of the force acting on the dislocation is composed of three parts: the dislocation image force f_{IE}, the force f_{AE} produced by nanoscale amorphization, and the force $f_{\Gamma\mathrm{E}}$ produced by an external load.

(1) The image force f_{IE} of the dislocation itself can be calculated by Peach–Koehler formula:

$$\begin{aligned}f_{IE} &= f_{IEx} - if_{IEy} = \left[\hat{\sigma}_{xy}(\zeta_0)b_x + \hat{\sigma}_{yy}(\zeta_0)b_y\right] + i\left[\hat{\sigma}_{xx}b(\zeta_0)_x + \hat{\sigma}_{xy}(\zeta_0)b_y\right]\\ &= \frac{\mu_1 b^2}{4\pi(1-\upsilon_1)}\left[\frac{\Phi_E^*(\zeta_0)+\overline{\Phi_E^*(\zeta_0)}}{\gamma_1} + \frac{\overline{\omega(\zeta_0)}\Phi_E^{*\prime}(\zeta_0)+\Psi_E^*(\zeta_0)}{\overline{\gamma}_1}\right],\end{aligned} \tag{22}$$

where $\hat{\sigma}_{xx}$, $\hat{\sigma}_{yy}$ and $\hat{\sigma}_{yy}$ are the interference stress field components, $\Phi_E^*(z_0) = \lim_{z\to z_0}\left[\Phi_1^E(z) - \Phi_{10}^E(z)\right]$, $\Phi_E^{*\prime}(z_0) = \lim_{z\to z_0}\frac{d\left[\Phi_1^E(z)-\Phi_{10}^E(z)\right]}{dz}$, $\Psi_E^*(z_0) = \lim_{z\to z_0}\left[\Psi_1^E(z) - \Psi_{10}^E(z)\right]$.

(2) The force f_{AE} acting on dislocations produced by nanoscale amorphization can be expressed as:

$$f_{AE} = b\sigma_{r\theta}^N = b\left[\left(\sigma_{yy}^N - \sigma_{xx}^N\right)\sin\theta\cos\theta + \sigma_{xy}^N\cos 2\theta\right], \tag{23}$$

where σ_{xx}^N, σ_{yy}^N and σ_{xy}^N are the components of the stress field produced by nanoscale amorphization.

(3) The calculation formula of the force $f_{\Gamma E}$ acting on the edge dislocation caused by the in-plane tensile load (model I) and the shear load (model II) acting at infinity can be expressed as:

$$f_{\Gamma E} = b\sigma_{r\theta}^{\Gamma} = \frac{b}{\sqrt{2\pi r_0}}\left(l_1 K_{\mathrm{I}}^N + l_2 K_{\mathrm{II}}^N\right), \tag{24}$$

where $l_1 = \frac{1}{2}\sin\theta_0\cos\frac{\theta_0}{2}$, $l_2 = \cos\frac{3\theta_0}{2} + \sin^2\frac{\theta_0}{2}\cos\frac{\theta_0}{2}$, K_{I}^N and K_{II}^N are the model I and model II stress intensity factors of the crack tip under infinite load.

Therefore, the emission force f_{E} acting on the edge dislocation can be written as:

$$f_E = f_{AE} + f_{IE} + f_{\Gamma E} = \mathrm{Re}[f_{AE} + f_{IE}]\cos\theta - \mathrm{Im}[f_{AE} + f_{IE}]\sin\theta + f_{\Gamma}. \tag{25}$$

5 Critical stress intensity factor corresponding to dislocation emission

J.S. Langer suggested that the second law of thermodynamics could be used to study the dynamics of dislocations, including strain hardening and elasticity, plastic yielding, shear banding, grain size effects, etc. [43, 44], and he found that the fracture toughness generally decreases as the temperature decreases [45–47].

This paper mainly studies the first dislocation emitted from the crack tip under constant temperature, without considering the influence of temperature change, so the dislocation emission criterion proposed by Rice and Tomson is adopted [48]. When the dislocation force on the dislocation is equal to zero, the dislocation will be emitted from the crack tip. Combining the formulas of dislocation image force $f_{\Gamma E}$, the force f_{AE} generated by nanoscale amorphization, the force $f_{\Gamma E}$ generated by the applied load, and the critical condition $f_E = 0$ for dislocation emission, the expression of the critical stress intensity factor K_{IC}^N and K_{IIC}^N corresponding to the dislocation emission can be obtained:

$$K_{II}^N = 0 \quad K_{IC}^0 = \frac{\sqrt{2\pi r_0}}{bl_1}(\mathrm{Im}[f_{IE} + f_{AE}]\sin\theta - \mathrm{Re}[f_{IE} + f_{AE}]\cos\theta), \tag{26}$$

$$K_I^N = 0 \quad K_{IIC}^0 = \frac{\sqrt{2\pi r_0}}{bl_2}(\mathrm{Im}[f_{IE} + f_{AE}]\sin\theta - \mathrm{Re}[f_{IE} + f_{AE}]\cos\theta). \tag{27}$$

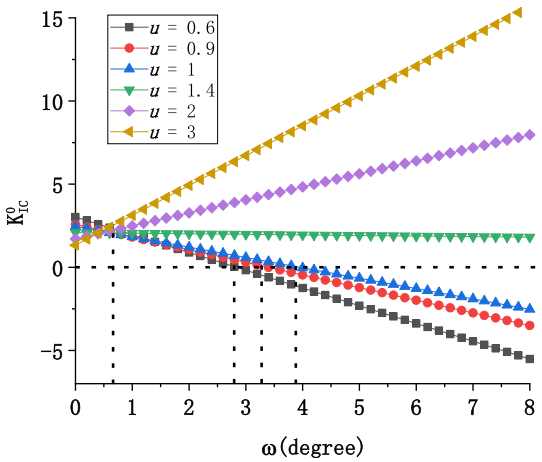

Fig. 3 Dependences of the critical normalized SIF K^0_{IC} on ω with different relative shear modulus u

6 Example analysis

According to the above formulas of critical stress intensity factors corresponding to dislocation emission, the influence of nanoscale amorphization and interface crack size in nanocrystalline bimaterials on the dislocation emission of collinear linear crack tips at the interface can be analyzed. In order to simplify the analysis, the critical stress intensity factors are dimensionless to $K^0_{IC} = K^N_{IC}/\mu_1\sqrt{b}$ and $K^0_{IIC} = K^N_{IIC}/\mu_1\sqrt{b}$, and the relative shear modulus of the upper and lower half planes is defined as $u = \mu_2/\mu_1$. And the dimensions of the nanoscale amorphized rectangular area are s and d, and $s = d$, the length of the interface crack is set to l, the material of the lower plane is assumed to be the nanocrystalline material 3C-SiC, and its parameters are: $\mu_2 = 217$ GPa, $\nu_2 = 0.23$. The strength of the wedge disclination is $\pm\omega$, and the first edge dislocation emitted from the interface crack is located in the upper half plane, let $b = 0.25$ nm and $r_0 = b/2$.

6.1 Influence of material constant and nanoscale amorphization strength

As shown in Fig. 3, when different relative shear modulus u, and $\alpha = 30°$, $r_1 = 0.15$ nm, $\theta_1 = 5°$, $\theta_0 = 9°$ $l = 2000$ nm, $d = 12$ nm, are taken, the model I critical stress intensity factor K^0_{IC} varies with disclination intensity ω. It can be seen from the figure that when the upper half plane is relatively hard, K^0_{IC} decreases with the increase in disclination intensity; when the upper half plane is relatively soft, K^0_{IC} increases with the increase in disclination intensity; and when the disclination strength is large (such as $\omega = 5°$), K^0_{IC} increases with the increase in the relative shear modulus u. On the contrary, when the disclination strength is small (such as $\omega = 1°$), K^0_{IC} decreases with the increase in relative shear modulus u. It can be seen that when the upper half plane is relatively hard, nanoscale amorphization deformation can hinder the dislocation emission at the tip of the interface crack; when the upper half plane is soft, the nanoscale amorphization deformation can promote the dislocation emission at the tip of the interface crack. When the upper half plane is relatively hard and the intensity factor is $K^0_{IC} = 0$, there is a critical disclination strength; at this time, the degree of nanoscale amorphization is most likely to promote the emission of crack tip dislocations, thereby showing the enhancement of the fracture toughness of the material. From Fig. 3, it can be known that the critical disclination strength value increases with the increase in the relative shear modulus u (when $u = 0.6$, $\omega_{\min} = 2.8$; when $u = 0.9$, $\omega_{\min} = 3.4$; when $u = 1$, $\omega_{\min} = 3.9$).

As shown in Fig. 4, it depicts the variation curve of the model I critical stress intensity factor K^0_{IC} with the relative shear modulus u when different disclination strengths ω and $\alpha = 30°$, $r_1 = 0.15$ nm, $\theta_1 = 5°$, $\theta_0 = 9°$, $l = 2000$ nm, $d = 12$ nm are taken. It can be seen from the figure that when there is no nanoscale amorphization deformation ($\omega = 0°$), K^0_{IC} decreases with the increase in relative shear modulus u and then tends to a stable value, indicating that interface cracks are prone to emit dislocations in a softer half plane; when considering the nanoscale amorphization deformation ($\omega \neq 0°$) near the interface crack, the curve of K^0_{IC} with the relative shear modulus u is more complicated. When the disclination strength is constant, there will be at least one relative shear modulus u_e that is easiest to emit. For example, when disclination intensity is $\omega = 1°$, $u_e = 0.9$,

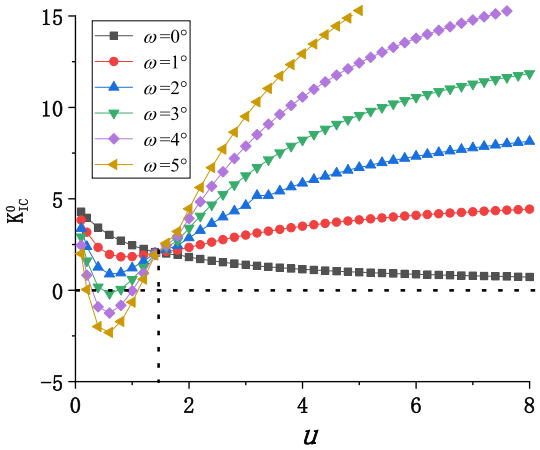

Fig. 4 Dependences of the critical normalized SIF K^0_{IC} on u with different disclination strengths ω

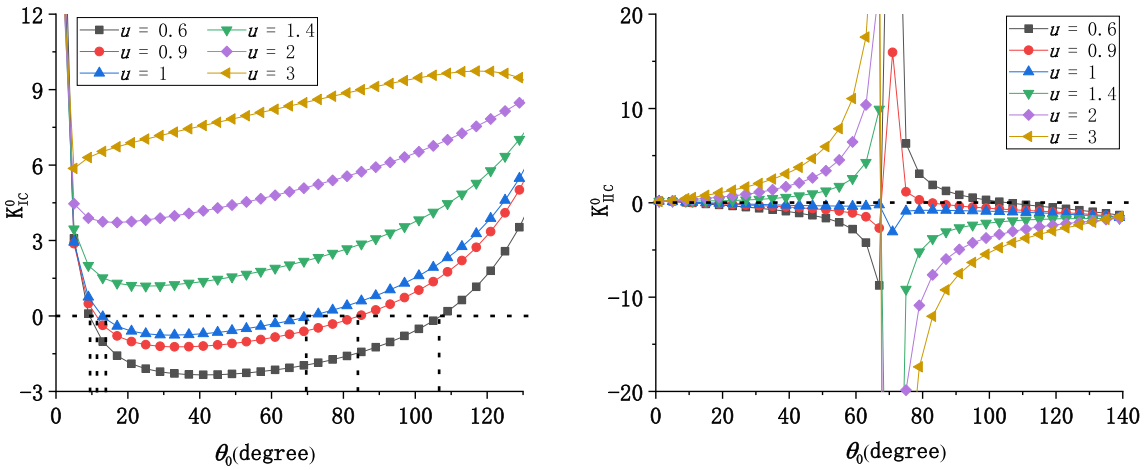

(a) K^0_{IC} **(b)** K^0_{IIC}

Fig. 5 Dependences of the critical normalized SIFs on the edge dislocation emission angle θ_0 with different relative shear modulus u for **a** K^0_{IC}; **b** K^0_{IIC}

when disclination intensity is $\omega = 2°, u_e = 0.7$; when disclination intensity is $\omega = 3°, u_e = 0.45, 0.8$; when disclination intensity is $\omega = 4°, u_e = 0.25, 1.0$; when disclination intensity is $\omega = 5°, u_e = 0.2, 1.1$. This will be consistent with the conclusion of the above figure that there will be critical disclination strength corresponding to most easily emitted dislocation only when the relative shear modulus $u < 1$.

6.2 Influence of dislocation emission angle

As shown in Fig. 5, when the relative shear modulus u is different, and $\omega = 3°, \alpha = 30°, r_1 = 0.15$ nm, $\theta_1 = 5°, l = 2000$ nm,$d = 12$ nm the model I and model II critical stress intensity factors K^0_C vary with the emission angle θ_0 of the edge dislocation.

It can be seen from Fig. 5a that K^0_{IC} decreases first and then increases with the increase in the dislocation emission angle, and there is a minimum value, which corresponds to the easiest dislocation emission angle θ_e. When the relative shear modulus is $u = 0.6$, the most probable dislocation launch angles are $\theta_e = 9.4°$ and 106.6°; when $u = 0.9, \theta_e = 12.6°$ and 82.5°; when $u = 1.0, \theta_e = 14.9°$, and 68.4°; When the relative shear modulus is $u = 1.4, \theta_e = 26.8°$; when $u = 2.0, \theta_e = 18.9°$; when $u = 3.0, \theta_e = 4.8°$.

It can be seen from Fig. 5b that K^0_{IIC} increases with the increase in the dislocation emission angle from a finite positive value to infinity (decreases to infinitesimal) and then changes to a negative value (positive value)

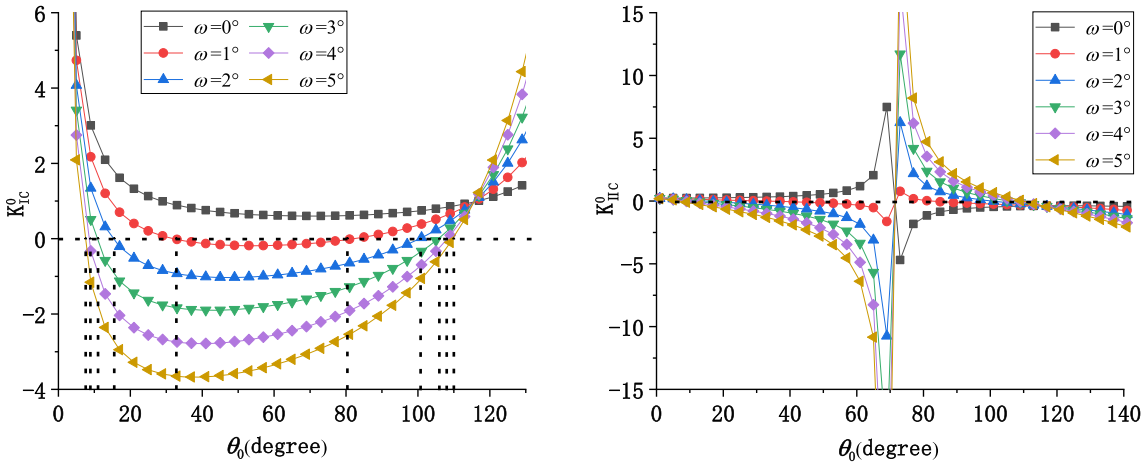

(a) K^0_{IC} **(b)** K^0_{IIC}

Fig. 6 Dependences of the critical normalized SIFs on the edge dislocation emission angle θ_0 with different disclination strengths ω for **a** K^0_{IC}; **b** K^0_{IIC}

and increases from an infinite negative value to a finite negative value because the sign of the critical stress intensity factor is determined by the direction of the Burger vector emitting dislocations. It can be seen that the most probable emission angle of a positive edge dislocation is 0°. $\left|K^0_{IIC}\right|$ increases first and then decreases with the increase in u.

As shown in Fig. 6, it depicts when the relative shear modulus $u = 0.6$, the disclination strength ω, and $\alpha = 30°$, $r_1 = 0.15$ nm, $\theta_1 = 5°$, $l = 2000$ nm, $d = 12$ nm are taken, the model I and model II critical stress intensity factor K^0_C varies with the emission angle θ_0 of the edge dislocation.

It can be seen from Fig. 6a that the model I critical intensity factor will first drop sharply with the increase in the dislocation emission angle, then stabilize, and finally rise sharply. Therefore, there will be a minimum value θ_e of the dislocation emission angle that dislocations are most easily emitted. When there is no nanoscale amorphization deformation $\omega = 0°$ at the crack tip, the most likely emission angle of the crack tip dislocation is $\theta_e = 70.85°$, However, when considering the nanoscale amorphization deformation ($\omega \neq 0°$) near the end of a straight crack, as the disclination strength ω increases, the most likely angle θ_e will decrease, For example, when disclination intensity is $\omega = 1°$, the emission angle is $\theta_e = 32.5°$, 80.4°; when disclination intensity is $\omega = 2°$, the dislocation emission angle is $\theta_e = 15.1°$, 98.8°; when disclination intensity is $\omega = 3°$, the dislocation emission angle is $\theta_e = 10.8°$, 104.7°; when disclination intensity is $\omega = 4°$, the emission angle is $\theta_e = 8.2°$, 107.9°; when disclination intensity is $\omega = 5°$, the emission angle is $\theta_e = 6.9°$, 108.8°.

It can be seen from Fig. 6b that when there is no nanoscale amorphization deformation ($\omega = 0°$) at the crack tip, the model II critical intensity factor K^0_{IIC} will, at first, gradually increase from a positive value approaching zero to a finite positive value with the increase in the dislocation emission angle, and then converted to a negative value, and with the increase in the dislocation angle, it eventually tends to a negative value near zero. It is found that the most likely emission angle when there is no nanoscale amorphization deformation at the crack tip is $\theta_e = 71.46°$. When considering the nanoscale amorphization deformation near the end of a straight crack ($\omega \neq 0°$), the model II critical intensity factor K^0_{IIC} will, at first, gradually decrease from a positive value tending to zero to a negative value of infinity as the dislocation emission angle increases, and then convert to a positive value, and with the increase in the dislocation angle, it eventually tends to a negative value near zero. Therefore, it can be seen from the figure that the crack tip dislocation launches at the most probable angle $\theta_e = 0°$.

6.3 Influence of grain size and inclination angles

As shown in Fig. 7, the model I critical stress intensity factor K^0_{IC} varies with different grain sizes d when,$\alpha = 30°$, $r_1 = 0.15$ nm, $\theta_1 = 5°$, $\theta_0 = 9°$, $l = 2000$ nm. In this analysis, the relative shear modulus is set to the u_e corresponding to different disclination strengths ω according to the above results, such as $u_e = 0.9$ when

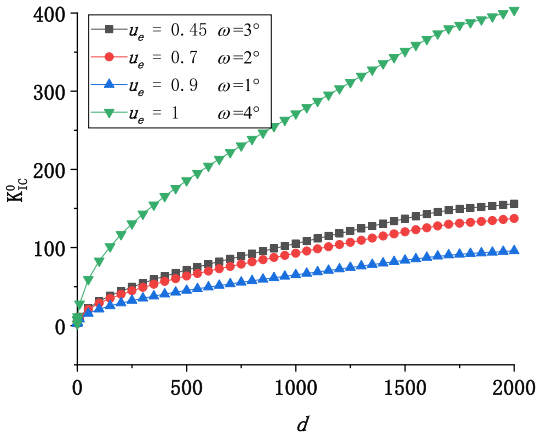

Fig. 7 Dependences of the critical normalized SIF K^0_{IC} on grain size d with different relative shear modulus u and disclination strengths ω

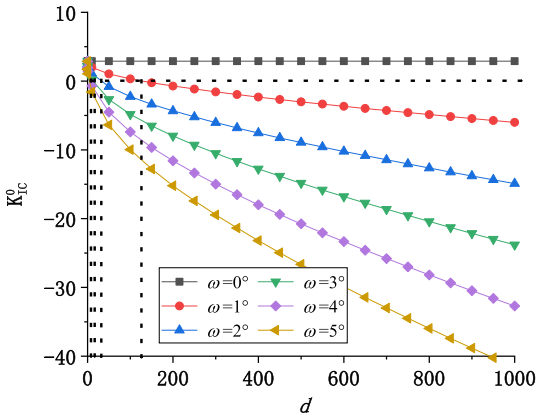

Fig. 8 Dependences of K^0_{IC} on grain size d with different disclination strengths ω

$\omega = 1°, u_e = 0.7$ when $\omega = 2°, u_e = 0.45$ when $\omega = 3°$, and $u_e = 1.0$ when $\omega = 4°$. It can be seen from the figure that K^0_{IC} increases with the increase in grain size d; and when the grain size d is constant and the relative shear modulus is $u = \frac{\mu_2}{\mu_1} < 1$, K^0_{IC} increases with the increase in disclination intensity ω, indicating that when the upper half plane is relatively soft, it is helpful for the emission of dislocations.

As shown in Fig. 8, the model I critical stress intensity factor K^0_{IC} varies with the grain size d when disclination strengths ω are different, and $u = 0.6, \alpha = 30°, r_1 = 0.15$ nm, $\theta_1 = 5°, \theta_0 = 9.4°, l = 2000$ nm. It can be seen from the figure: (1) when the grain size is constant, K^0_{IC} increases with the increase in disclination strength ω, which is consistent with the conclusions of Figs. 3 and 4; (2) when there is no nanoscale amorphization ($\omega = 0°$) at the crack tip, the critical stress intensity factor K^0_{IC} is a fixed value. When considering the existence of nanoscale amorphization ($\omega \neq 0°$) near the end of the linear crack, the critical stress intensity factor will decrease as the grain size d increases, and there is a critical grain size d_0 that makes $K^0_{IC} = 0$; as long as the grain size $d > d_0$, dislocations can be emitted at the tip of the interface crack without external load; the critical grain size d_0 decreases as the disclination strength ω increases.

As shown in Fig. 9, it depicts when taking different disclination dipole arm inclination angles α, and $u = 0.6$, $\omega = 3°$, $r_1 = 0.15$nm,$\theta_1 = 5°, \theta_0 = 9.4°$, $l = 2000$nm, the model I critical stress intensity factor K^0_{IC} varies with the grain size d. It can be seen from the figure that when the tilt angle of the disclination dipole arm is $\alpha \leq 10°$, the K^0_{IC} stress intensity factor first increases and then decreases with the increase in the grain size; when the tilt angle of the disclination dipole arm is $\alpha > 10°$, the K^0_{IC} stress intensity factor decreases with the increase in the grain size. As the tilt angle α of the disclination dipole arm increases, there is a critical grain size d_0 for $K^0_{IC} = 0$, and d_0 decreases as the tilt angle α of the disclination dipole arm increases.

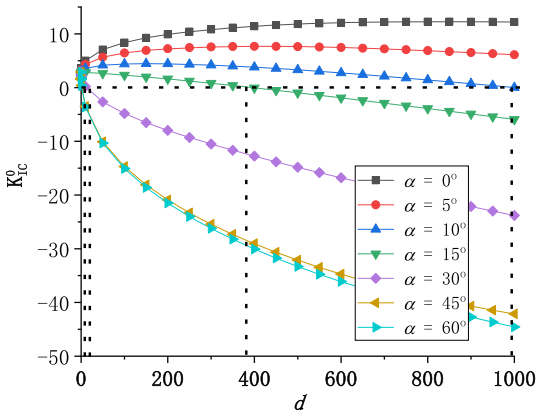

Fig. 9 Dependences of K^0_{IC} on grain size d with different disclination dipole arm inclination angles α

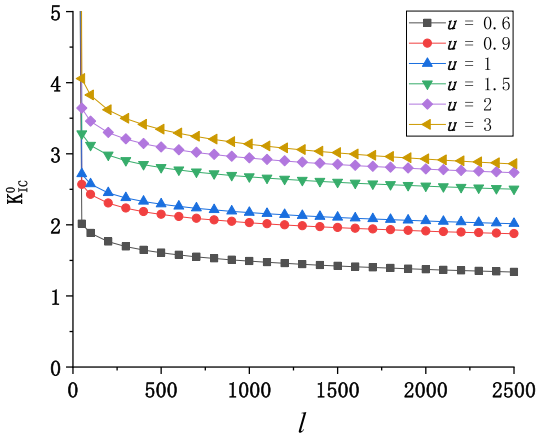

Fig. 10 Dependences of the critical normalized SIF K^0_{IC} on crack length l with different relative shear modulus u

6.4 Influence of crack length

Figure 10 depicts the variation law of model I and model II critical stress intensity factor K^0_C with crack length l when different relative shear modulus u, and $\omega = 3°$, $\alpha = 30°$, $r_1 = 0.15$ nm, $\theta_1 = 5°, \theta_0 = 9°$, $d = 12$ nm, are used. It can be seen from the figure that K^0_{IC} decreases with increasing crack length l; when the crack length is constant, K^0_{IC} increases with increasing relative shear modulus.

As shown in Fig. 11, when the disclination strength ω, and $u = 0.6$, $\alpha = 30°$, $r_1 = 0.15$nm, $\theta_1 = 5°$, $\theta_0 = 9.4°$, $d = 12$ nm are taken, the model I critical stress intensity factor K^0_{IC} varies with the crack length l. It can be seen from the figure that when there is no nanoscale amorphization ($\omega = 0°$) near the crack tip, K^0_{IC} first decreases sharply and then slowly decreases with increasing crack length l; when considering the existence of nanoscale amorphization ($\omega \neq 0°$) near the end of a linear crack, the K^0_{IC} critical stress intensity factor will first increase sharply and then slowly decrease as the crack length l increases. When the crack length is constant, K^0_{IC} decreases with increasing disclination strength ω, which is consistent with the previous conclusion.

7 Conclusion

In summary, this paper establishes a theoretical model of analyzing the influence of nanoscale amorphization on dislocation emission from collinear line crack tip at the interface in nanocrystalline bimaterials. Using the complex potential method of elastic mechanics, the complex potential function solution of the built model is obtained, and the law of the influence of nanoscale amorphization and interfacial crack size on the dislocation

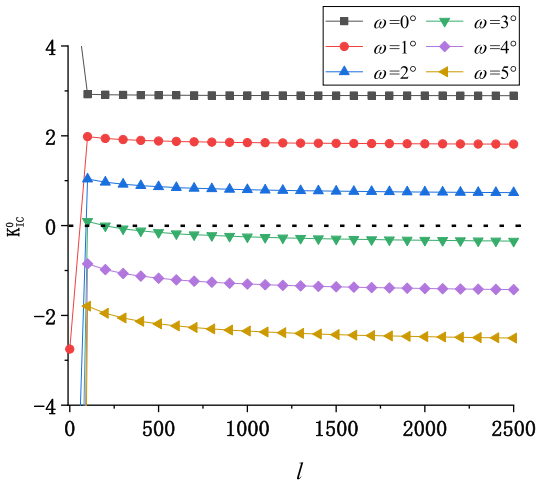

Fig. 11 Dependences of K_{IC}^{0} on crack length l with different disclination strengths ω

emission at the tip of interfacial cracks is analyzed by using calculation examples, and the toughness changes of nanocrystalline dual materials containing defects due to dislocation emission are also discussed.

1. When the material is relatively soft, the interface crack is easy to emit dislocations. And the appropriate selection of materials for the upper and lower planes can reduce the critical stress intensity factor related to dislocation emission, thereby promoting the dislocation emission of interface cracks and improving the toughness of the nanocrystalline bimaterials.
2. When the upper half-plane is relatively hard, nanoscale amorphization can promote dislocation emission at the tip of the interface crack; when the upper half-plane is soft, nanoscale amorphization can hinder the dislocation emission at the tip of the interface crack. And the existence of nanoscale amorphization promotes the dislocation emission at the tip of the interface crack in the case, which improves the toughness of the material due to dislocation emission.
3. When the upper half plane is relatively hard, the most probable dislocation emission angle increases with the increase in the relative shear modulus; when the upper half plane is relatively soft, the most probable emission angle of dislocations decreases with the increase in relative shear modulus; and the most probable emission angle of dislocations decreases with the increase in disclination intensity. The most likely emission angle for a positive edge dislocation is 0°, and the absolute value of the critical stress intensity factor increases with the increase in the relative shear modulus.
4. There is a critical grain size making the dislocation emission from the crack tip most easily. And the critical grain size decreases with the increase in the wedge disclination inclination angle. Therefore, when the upper half plane where the dislocation is located is relatively soft, it is helpful for the emission of the dislocation.

Acknowledgements The authors would like to deeply appreciate the support from the Natural Science Foundation of Hunan Province (2021JJ31136), the key scientific research projects of Hunan Provincial Education Department (20A522), the National Natural Science Foundation of China (11602308) and the science and technology innovation Program of Hunan Province (2020RC4049).

References

1. Kuntz, J.D., Zhan, G.D., Mukherjee, A.K.: Nanocrystalline-matrix ceramic composites for improved fracture toughness. MRS Bull. **29**, 22–27 (2004)
2. Yang, F., Yang, W.: Crack growth versus blunting in nanocrystalline metals with extremely small grain size. J. Mech. Phys. Solids **57**, 305–324 (2009)
3. Barai, P., Weng, G.J.: Mechanics of creep resistance in nanocrystalline solids. Acta Mech. **195**, 327–348 (2008)
4. Mukhopadhyay, A., Basu, B.: Consolidation–microstructure–property relationships in bulk nanoceramics and ceramic nanocomposites: a review. Int. Mater. Rev. **52**, 257–288 (2007)
5. Ovid'Ko, I.A.: Deformation and Diffusion Modes in Nanocrystalline Materials. Int. Mater. Rev. **50**, 65–82 (2005)

6. Figueiredo, R.B., Kawasaki, M., Langdon, T.: The mechanical properties of ultrafine-grained metals at elevated temperatures. Rev. Adv. Mater. Sci **19**, 1–12 (2009)
7. He, T., Feng, M., Chen, X.: Martensitic Transformation Effect on the Dislocation Emission from a Semi-infinite Crack Tip in Nanocomposites. Acta Mech. Solida Sin. **32**(2), 160–172 (2019)
8. Sun, X., Han, W., Liu, Q., Hu, P., Hong, C.: ZrB2-ceramic toughened by refractory metal Nb prepared by hot-pressing. Mater Des. **31**(9), 4427–4431 (2010)
9. Zhu, Y.F., Shi, L., Liang, J., Hui, D., Lau, K.T.: Synthesis of zirconia nanoparticles on carbon nanotubes and their potential for enhancing the fracture toughness of alumina ceramics. Compos Part B Eng. **39**(7–8), 1136–1141 (2008)
10. Li, M., Schaffer, H., Soboyejo, W.O.: Transformation toughening of NiAl composites reinforced with yttria partially stabilized zirconia particles. J Mater Sci. **35**(6), 1339–1345 (2000)
11. Zhao, H.B., Feng, H., Liu, F., et al. Effect of nanoscale twin and dislocation pileup at twin boundary on crack blunting in nanocrystalline materials. Acta Mech. (2017).
12. Yu, M., Yang, Y., Peng, X., et al.: Effect of nanotwin and dislocation pileup at twin boundary on dislocation emission from a semi-elliptical blunt crack tip in nanocrystalline materials. Eng. Fract. Mech. **202**, 288–296 (2018)
13. Ovid'ko, I.A., Sheinerman, A.G., Aifantis, E.C.: Effect of cooperative grain boundary sliding and migration on crack growth in nanocrystalline solids. Acta Mater. **59**, 5023–5031 (2011)
14. Li, J., Jin, Z.Q., Liu, J.P., Wang, Z.L., Thadhani, N.N.: Amorphization and ultrafine-scale recrystallization in shear bands formed in shock-consolidated Pr2Fe14B/α-Fe nanocomposite magnets. Appl. Phys. Lett. **85**, 2223–2225 (2004)
15. Wang, Y.M., Bringa, E.M., McNaney, J.M., Victoria, M., Caro, A., Hodge, A.M., Smith, R., Torralva, B., Remington, B.A., Schuh, C.A., Jamarkani, H., Meyers, M.A.: Deforming nanocrystalline nickel at ultrahigh strain rates. Appl. Phys. Lett. **88**, 061917 (2006)
16. Clayton, J.D., Knap, J.: Continuum modeling of twinning, amorphization, and fracture: theory and numerical simulations. Continuum Mech. Thermodyn. **30**, 421–455 (2017)
17. Bobylev, S., Ovid'ko, I.: Nanoscale amorphization at disclination quadrupoles in deformed nanomaterials and polycrystals. Appl. Phys. Lett. **93**, 061904 (2008)
18. Ovid'ko, I.: Nanoscale amorphization as a special deformation mode in nanowires. Scr. Mater. **66**, 402–405 (2012)
19. Nagumo, M., Ishikawa, T., Endoh, T., Inoue, Y.: Amorphization associated with crack propagation in hydrogen-charged steel. Scripta Mater. **2012**(49), 837–842 (2003)
20. Zhu, Y.T., Liao, X.Z., Wu, X.L.: Deformation twinning in bulk nanocrystalline metals: experimental observations. JOM. **60**, 60 (2008)
21. Wu, X.L., Zhu, Y.T.: Partial-dislocation-mediated processes in nanocrystalline Ni with nonequilibrium grain boundaries. Appl. Phys. Lett. **89**, 58 (2006)
22. Wang, Y.M., Hodge, A.M., Biener, J., Hamza, A.V.: Deformation twinning during nanoindentation of nanocrystalline Ta. Appl. Phys. Lett. **86**, 44 (2005)
23. Fang, Q., Zhang, L., Liu, Y.: Influence of grain boundary sliding and grain size on dislocation emission from a crack tip. Int. J. Damage Mech. **23**, 192–202 (2013)
24. Fang, Q.H., Feng, H., Liu, Y.W., Lin, S., Zhang, N.: Special rotational deformation effect on the emission of dislocations from a crack tip in deformed nanocrystalline solids. Int. J. Solids Struct. **49**, 1406–1412 (2012)
25. Chen, B.T., Lee, S.: Dislocation emission criterion for a wedge crack under mixed mode loading. Int. J. Fract. **102**, 287–302 (2000)
26. Zhou, K., Wu, M.S., Nazarov, A.A.: Relaxation of a disclinated tricrystalline nanowire. Acta Mater. **56**, 5828–5836 (2008)
27. Fang, Q.H., Liu, Y., Liu, Y.W., Huang, B.Y.: Dislocation emission from an elliptically blunted crack tip with surface effects. Physica B **404**, 3421–3424 (2009)
28. Feng, H., Fang, Q.H., Liu, Y.W., Chen, C.P.: Nanoscale rotational deformation effect on dislocation emission from an elliptically blunted crack tip in nanocrystalline materials. Int. J. Solids Struct. **51**, 352–358 (2014)
29. Feng, H., Fang, Q.H., Zhang, L.C., Liu, Y.W.: Effect of cooperative grain boundary sliding and migration on emission of dislocations from a crack tip in nanocrystalline materials. Mech. Mater. **61**, 39–48 (2013)
30. Ovid'ko, I.A., Sheinerman, A.G.: Ductile vs brittle behavior of pre-cracked nanocrystalline and ultrafine-grained materials. Acta Mater. **58**(16), 5286–5294 (2010)
31. Lyu, D., Li, S.: Recent developments in dislocation pattern dynamics: current opinions and perspectives. J. Micromech. Mole. Phys. (2018).
32. Fang, Q.H., Zhang, L.C.: Coupled effect of grain boundary sliding and dislocation emission on fracture toughness of nanocrystalline materials. J. Micromech. Mole. Phys. **01**(02), 1650008 (2016)
33. Zhou, K., Wu, M.S.: Elastic fields due to an edge dislocation in an isotropic film-substrate by the image method. Acta Mech. **211**(3–4), 271–292 (2010)
34. Lee, S.L., Huang, W.S., Shiue, S.T.: Elastic interaction between screw dislocations and a blunting interfacial crack. Mater. Sci. Eng., A **142**(1), 41–50 (1991)
35. Fang, Q., Liu, Y., Jiang, C.: Interaction between a screw dislocation and an elastic elliptical inhomogeneity with interfacial cracks. Acta. Mech. Sin. **21**(002), 151–159 (2005)
36. Junjie, Q., Rongjia, L.: Analysis of interface crack stress and electric field concentration factor of thin film substrate structure. Chin. J. Appl. Mech. **37**(163), 362–368 (2020)
37. Zhang, S., Yao, H., Li, J.: Stress fields near mode II interface crack tip of two dissimilar orthotropic composite materials. Key Eng. Mater. **385–387**, 585–588 (2008)
38. Huijuan, Z., Anqiang, D., Junlin, Li., et al.: Stress analysis of anti-plane interface cracks in orthotropic piezoelectric bimaterials. J. Taiyuan Univ. Sci. Technol. **041**(001), 72–77 (2020)
39. Hirth, J.P., Lothe, J.: Theory of Dislocations, 2nd edn. John-wiley, New York (1964)
40. Mushkelishvili, N.I.: Some Basic Problems of Mathematical Theory of Elasticity (1975).
41. Fang, Q.H., Liu, Y.W., Jiang, C.P., et al.: Interaction of a wedge disclination dipole with interfacial cracks. Eng. Fract. Mech. **73**(9), 1235–1248 (2006)

42. Zhang, T.Y., Li, J.: Interaction of an edge dislocation with an interfacial crack. J. Appl. Phys. **72**(6), 2215 (1992)
43. Langer, J.S.: Fracture toughness of crystalline solids. Phys. Rev. E **103**(6), 063004 (2021)
44. Langer, J.S., Le, K.C.: Scaling confirmation of the thermodynamic dislocation theory. Proc. Natl. Acad. Sci. **117**(47), 29431–29434 (2020)
45. Le, K.C., Tran, T.M., Langer, J.S.: Thermodynamic dislocation theory of adiabatic shear banding in steel. Scripta Mater. **149**, 62–65 (2018)
46. Issa, I., Hohenwarter, A., Fritz, R., et al.: Fracture properties of ultrafine grain chromium correlated to single dislocation processes at room temperature. J. Mater. Res. **34**(13), 2370–2383 (2019)
47. Youssef, K.M., Scattergood, R.O., Murty, K.L., Koch, C.C.: Nanocrystalline Al–Mg alloy with ultrahigh strength and good ductility. Scripta Mater. **54**, 251–256 (2006)
48. Rice, J.R., Thomson, R.: Ductile versus brittle behavior of crystals. Philos. Mag. **29**, 73–80 (1974)